Modelling the effects of the mountain pine beetle on snowmelt in a subalpine forest

Danielle Perrot,[1]* Noah P. Molotch,[1,2] Keith N. Musselman[3] and Evan T. Pugh[4]

[1] *Department of Geography, Institute of Arctic and Alpine Research, University of Colorado at Boulder, Boulder, CO, USA*
[2] *Jet Propulsion Laboratory, California Institute of Technology, Pasadena, CA, USA*
[3] *Department of Civil and Environmental Engineering, University of California, Los Angeles, Los Angeles, CA, USA*
[4] *Department of Geology, University of Colorado at Boulder, Boulder, CO, USA*

ABSTRACT

The recent mountain pine beetle epidemic in the Colorado River Basin has resulted in widespread tree mortality in pine stands across the Colorado Plateau. Because of complex micro-scale (i.e. tree well scale) interactions between vegetation and snow processes, one of the most significant issues resulting from this epidemic is the potential hydrologic impacts of the effects of changing forest structure. Using SNTHERM, we conducted a comparative modelling scenario analysis of the snowpack along a transect between two trees over the course of the snow ablation season (28 February–30 June) under four forest stand conditions to assess changes in snowpack characteristics because of loss of canopy biomass. We found that the red phase scenario (intermediate phase of tree death) exhibited a 4-day earlier snow disappearance date than the living stand scenario and grey phase scenario (advanced phase of tree death), although the timing of isothermal conditions at $0\,^{\circ}$C was identical. The modelled clearcut scenario snowpack became isothermal at $0\,^{\circ}$C 10 days earlier than the living, red phase, or grey phase scenarios. The clearcut modelling scenario also exhibited the greatest homogenization of snow properties, and the spatio-temporal distribution of snow disappearance at the tree well scale was 70% as variable as the living, red phase and grey phase modelling scenarios. These results provide insight to the processes responsible for changing hydrologic dynamics in snow-dominated forest ecosystems with the onset of vegetation stress and death and may help inform future forest management strategies. Copyright © 2012 John Wiley & Sons, Ltd.

KEY WORDS   snow–vegetation interactions; mountain pine beetle; snowmelt modeling; tree death

Received 16 April 2012; Revised 11 September 2012; Accepted 12 September 2012

INTRODUCTION

The hydrology and ecology of subalpine regions are sensitive to variations in climate and associated changes to the seasonal snowpack (Westerling *et al.*, 2006). A recent large-scale bark beetle outbreak has greatly affected the vegetation composition, structure and hydrologic dynamics of 600 000 km^2 of coniferous forests in western North America (Bentz *et al.*, 2009). In Colorado alone, the mountain pine beetle (*Dendroctonus ponderosae*, MPB) has impacted more than two-thirds of the state's lodgepole pine stands, a region that is approximately 6000 km^2 or two-fifths of Colorado's forestlands (Bentz *et al.*, 2009). Areas of coniferous vegetation susceptible to bark beetle outbreak are often located at subalpine elevations that experience a seasonal snowpack. This serves as a significant contributor to streamflow and water resources in the Western US (Bales *et al.*, 2006).

Bark beetles cause widespread and rapid tree death and result in a profound change in the canopy structure of forest stands. MPB-affected conifer stands can be characterized by two phases of mortality. In the first stage, often termed

'red phase', needles change from green to red in colour and drop from the canopy to the ground surface at a rate faster than the normal litterfall of a living stand (Wulder *et al.*, 2006). For lodgepole pine (*Pinus contorta*), this phase occurs approximately 2–4 years after the initial infestation. The secondary stage of death, termed the 'grey phase', occurs 5–20 years after the initial infestation and is characterized by a stand that has lost most or all of its needles and small twigs and branches (Wulder *et al.*, 2006). Salvage harvesting is a common forest management treatment for MPB-affected stands (Jenkins *et al.*, 2008) and can result in clearcut areas.

In subalpine forests, snowpack processes are determined in part by the canopy structure (Hedstrom and Pomeroy, 1998; Musselman *et al.*, 2008; Molotch *et al.*, 2009; Veatch *et al.*, 2009), and thus, changes in forest structure associated with changes in stand health may alter the timing and magnitude of snowmelt. Snow–vegetation interactions in coniferous forests have been thoroughly studied since the mid-20th century; it has been well established that stem density, canopy density and leaf area index influence snowpack energy and mass balance (for a review, see Varhola *et al.*, 2010). In coniferous forests, seasonal maximum snow accumulation occurs in canopy gaps, with reduced snow depths under the canopy and seasonal minimum depths in close proximity to tree boles (i.e. tree wells) (Faria *et al.*, 2000; Sicart *et al.*, 2004;

*Correspondence to: Danielle Perrot, Department of Geography, University of Colorado at Boulder, Institute of Arctic and Alpine Research Campus, Box 450, Boulder, CO 803, USA.
E-mail: danielle.perrot@colorado.edu

Musselman *et al.*, 2008). The micro-scale interactions between canopy and snowpack processes can be characterized by the tree well concept. This conceptual model hypothesizes that within a stand, differences in snow depth and other snow characteristics are a function of differences in incident precipitation and energy to the snowpack relative to tree boles (Faria *et al.*, 2000; Sicart *et al.*, 2004). Molotch *et al.* (2009) found that snow accumulation in open areas was 29% greater than that of mixed-conifer forested areas (lodgepole pine and Engelmann spruce dominated); Musselman *et al.* (2008) found snow ablation rates to be 54% greater in open versus under canopy conditions in a mixed-conifer forest (Douglas fir, white fir and blue spruce dominated) and found strong correlation between micro-scale canopy structure parameters and snow depth. The distribution of snow depth influences the distribution of snowpack properties (Faria *et al.*, 2000; Sicart *et al.*, 2004) as well as other environmental conditions such as soil temperature and soil moisture. Thus, the tree well concept can be extended in its relevance beyond hydrologic processes to forest biogeochemistry and microbial activity (Monson *et al.*, 2006).

Given the strong influence of the canopy on snow processes, it is implicit that a change in canopy structure should produce a change in snowpack characteristics. Numerous studies have been conducted to characterize runoff generation and/or snow processes at the stand scale under MPB-related vegetation change (Bethlahmy, 1974, 1975; Potts, 1984; Boon, 2007, 2009; Pomeroy *et al.*, 2008; Lewis and Huggard, 2010; Winkler *et al.*, 2010; Pugh and Small, 2011, 2012; Pugh and Gordon, 2012). In British Colombia (BC), Boon (2009) observed that snow ablation rates in a beetle kill forest plot were higher compared with those in the healthy plot but lower than the ablation rates in a clearcut plot. Pugh and Small (2011) observed that red phase stands experience melt out dates as much as 7 days before living stands. These previous studies have focused on changes in snow properties at the stand level, although the distribution of snow properties in forested regions likely exhibits considerable intra-stand spatial variability.

This study investigates the micro-scale processes driving changes in snow properties associated with tree mortality through a comparative modelling scenario analysis. First, we designated a total of four classes of modelling scenarios: three scenarios related to canopy structure under MPB-related tree mortality (living, red phase and grey phase) and an MPB management scenario (clearcut). Second, we made detailed above canopy meteorological measurements and collected snowpack data along a tree-to-tree snow trench in a living stand. As measurements were not made in red phase, grey phase or clearcut stands, we use canopy-related parameterizations of model forcing data to simulate snowpack conditions under the different scenarios. We estimated sub-canopy shortwave radiation, longwave radiation, wind speed, snow surface albedo and canopy snow interception for our four modelling scenarios according to canopy characteristics representative of living, red phase, grey phase and clearcut stands. These meteorological variables were used as forcing for the snowmelt model SNTHERM (Jordan, 1991). We used the snowpack measurements collected in the living stand to initialize SNTHERM in early March for all four modelling scenarios. We applied SNTHERM in a one-dimensional manner at multiple locations along a horizontal tree-to-tree snow transect to estimate changes in snow properties from 01 March to 30 June under different theoretical stand conditions. Relative differences in modelled distributions of snow density, snow grain size and temperature at the scale of the tree well can reveal the role of canopy changes with respect to the spatio-temporal distribution of snowmelt. We address two primary research questions: First, how do differences in canopy structure influence snow ablation dynamics? Second, how do differences in canopy structure affect the spatial distribution of snow properties at the tree well scale?

STUDY AREA

Snowpack and meteorological data were collected at the Niwot Ridge Long Term Ecological Research Site, Colorado, USA (40°1′58′′N; 105°32′47′′W), located on the east side of the Continental Divide at 3050 m above sea level (Figure 1). The climate is typical of a continental subalpine site in the western US, with the majority of precipitation falling as snow during the winter months. The forest is composed of mixed stands of living subalpine fir (*Abies lasiocarpa*), Engelmann spruce (*Picea engelmanii*) and lodgepole pine (*Pinus contorta*). The site has a long history of field studies related to the hydrology and ecology of subalpine forests (e.g. Bowling *et al.*, 2009; Molotch *et al.*, 2009; Monson *et al.*, 2010). Detailed observations of above canopy energy exchange, CO_2 and H_2O vapour fluxes have been made by a flux tower at the site as part of the Ameriflux network.[1] In addition, the site is within the University of Colorado Mountain Research Station's Climate Program, which provides hydrometric measurements at the nearby C-1 climate station with a record dating back to 1952. The site is also outfitted with detailed snowpack instrumentation (Figure 1) and has a nearby Natural Resources Conservation Service Snowpack Telemetry station.

FIELD METHODS

To reveal the effects of diminished canopy on the spatial distribution of snow properties and snowmelt, we utilized a detailed set of snow–vegetation measurements and meteorological measurements in a living stand to initialize and force the snowmelt model SNTHERM (Jordan, 1991) at discrete locations along a tree-to-tree snowpack transect. We do not have measurements in red phase, grey phase or clearcut stands. Our *in situ* measurements included the following: (1) micro-scale observations of horizontal and vertical variabilities in physical snow properties along a tree-to-tree trench dug in the snow (i.e. snow grain size, snow temperature and snow density); (2) automated snow

---

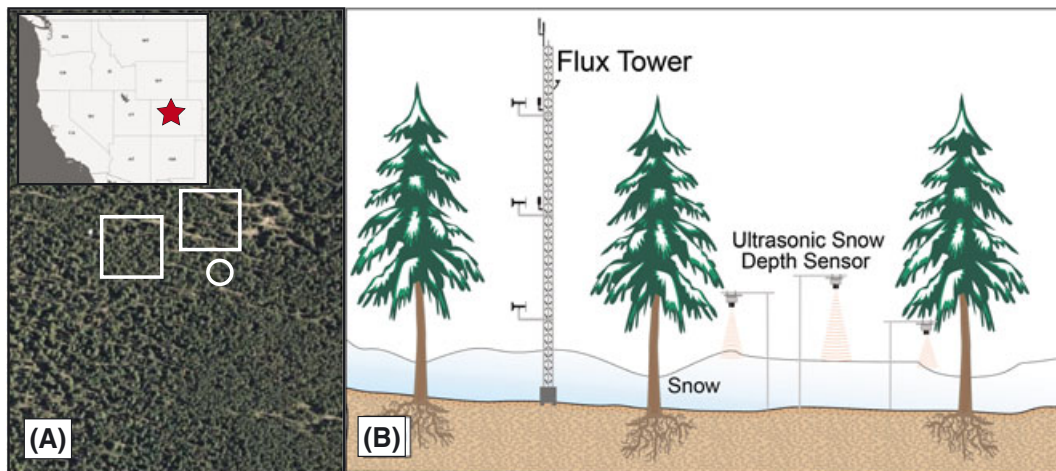[1]http://spot.colorado.edu/~monsonr/Ameriflux.html

Figure 1. (A) Location of snow and meteorological observations, Niwot Ridge, Colorado, USA. (B) Location of snow depth clusters (squares) (also the location of the tree-to-tree snow trench) and flux tower (circle) at Niwot Ridge. (C) Representation of instrument setup.

depth sensors placed at locations under the canopy, at the canopy edge and in canopy openings; and (3) meteorological measurements (i.e. air temperature, wind speed, solar radiation, longwave radiation and relative humidity) that were used to force the snowmelt model. These measurements are described in detail in the following text.

Tree-to-tree snow trench measurements

We used snowpack data collected on 28 February 2006 at Niwot Ridge for model initialization. A snow trench adjacent to a flux tower was dug along an east–west oriented tree-to-tree transect, with a total horizontal distance of 298 cm (white grid in Figure 2). Vertical profile measurements of snow characteristics were made at discrete locations along this transect at 25, 75 and 149 cm from the east tree and at 25 and 75 cm from the west tree. This resulted in detailed snow stratigraphy profiles along a canopy gradient (i.e. under canopy, canopy edge and canopy gap locations). For each vertical profile, hardness
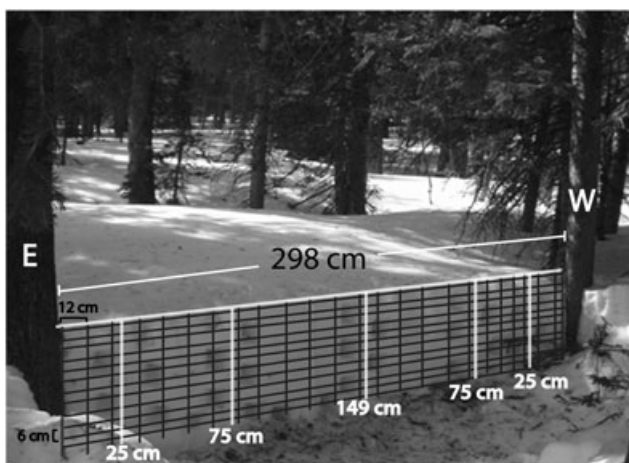

Figure 2. Snow trench at Niwot Ridge. The spatial resolution of snow density, snow temperature and hand lens grain size measurements are shown by the white vertical lines. The black grid depicts the spatial resolution of the spectral grain size measurements. Snow temperature and density values were interpolated to match the spatial resolution of the spectral grain size measurements. SNTHERM simulations were performed for each column on the black grid.

tests were conducted to identify snow layers. Then, for each layer, snow grain size and grain type data were collected using a hand lens with an 8×30 magnification. Snow temperature measurements were made for each layer by using a dial stem thermometer at 10 cm vertical intervals including the snow–atmosphere and snow–ground interfaces. Snow density measurements were also made at 10 cm vertical increments by using a $1000 \, cm^3$ stainless steel density cutter.

Hand lens grain size measurements are quite sensitive to observer subjectivity (Painter *et al*., 2007). Therefore, additional detailed snow grain size measurements were made using an ASD-Field Spectroradiometer (Boulder, Colorado) at a horizontal resolution of 12 cm and vertical resolution of 6 cm (black grid in Figure 2). This provided an extremely detailed characterization of vertical and horizontal variabilities in snow micro-structure. Whereas a hand lens is used to measure the geometric grain radius (GGR), the spectroradiometer measures the optical grain radius (OGR) as a function of the reflected spectral signature of measured grains (Painter *et al*., 2007). We translated our OGR values to GGR values by developing an empirical relationship between spectral grain radii and hand lens grain radii at corresponding depths.

The measured density and temperature values were then interpolated across the tree-to-tree trench to match the finer spatial resolution of the grain size measurements (black grid in Figure 2). To accomplish this, snow layers defined in the snow hardness tests were used to identify corresponding snow layers between the five measurement profiles (Figure 2, vertical white lines). Linear interpolation was performed in both the horizontal and vertical directions, to preserve characteristic snowpack layering. From this, we derived values for grain size and estimated values for temperature and density at discrete locations at a 12×6 cm interval across the tree-to-tree transect (Figure 2, black line grid). This resulted in 21 vertical profiles that were used to initialize 21 different SNTHERM simulations corresponding to different positions along the tree-to-tree transect. Additional snowpack data were also collected in the same manner on 24 March, 19 April and 17 May and were used for model performance assessment.

Snow depth measurements

To characterize amounts of spatially distributed snow interception and precipitation, nine ultrasonic snow depth sensors (Judd Communications) made hourly snow depth measurements in the stand; this array is described in detail by Molotch *et al.* (2009). Three locations along a canopy gradient were designated corresponding to proximity to tree bole: under canopy, canopy edge and open. Under canopy (under) corresponded to areas of full canopy presence, such that no branch ends were located directly overhead. Canopy edge (edge) had branch ends and some visible sky directly overhead such that these locations could be susceptible to canopy interception, unloading and throughfall during storms. Open locations corresponded to canopy gaps, such that no canopy was directly overhead. Three depth sensors were placed at each location defined by these three canopy configurations. The use of data from these sensors is described in the Modelling Methods section.

Continuous measurements of meteorological conditions

Meteorological data for 2006 were collected from a flux tower at the Niwot Ridge Long Term Ecological Research Site, which provides information about numerous meteorological variables including wind speed, air temperature, relative humidity, precipitation and incoming and outgoing shortwave and longwave radiation at 30-min time intervals (Table I). Methods used to translate above canopy measurements to sub-canopy model forcing data are described in the Modelling Methods section.

MODELLING METHODS

We used the snowmelt model SNTHERM (Jordan, 1991) to simulate physical snow properties at discrete locations along the snow transect from 1 March to 30 June for the theoretical scenarios of living, red phase, grey phase and clearcut stands. Energy exchange at the snow–atmosphere interface in SNTHERM is driven by meteorological conditions. Because SNTHERM lacks a canopy sub-model, above canopy meteorological data must be scaled to the sub-canopy as a function of canopy parameters. We estimated sub-canopy shortwave and longwave irradiance and wind speed with respect to stand canopy parameters for each stand scenario. We also parameterized snow albedo for each scenario and estimated incident precipitation with respect to location along the snow transect and the stand canopy parameters for each scenario. These procedures are described in detail in the following text. The sub-canopy estimates were then used to drive SNTHERM at 21 discrete locations along the tree-to-tree transect (at the measurement locations along the snow trench) for the living, red phase, grey phase and clearcut stand scenarios.

Snowmelt model: SNTHERM 89

SNTHERM is a process-driven, one-dimensional energy and mass balance snowmelt model that uses hydrometeorological variables to instigate change in 20 snow state variables (Jordan, 1991). Net fluxes of energy, mass and momentum drive the distribution of those same variables in the snowpack over the course of the modelling period. SNTHERM incorporates the principles of compaction, metamorphism and changes in snow depth to force changes in the number of layers, snow grain size and snow density values. Atmospheric forcings including relative humidity, air temperature, wind speed, incident shortwave radiation, incident longwave radiation and precipitation provide SNTHERM necessary information for estimating snowpack states such as grain size, snow temperature, snow density and layering at an hourly time interval over the period for which meteorological data are provided.

To simulate snowpack dynamics along the tree-to-tree transect, we initialized SNTHERM with 21 vertical profiles of snow properties collected in a living phase stand as described previously in Field Methods section. All modelling scenarios were initialized with the same snowpack observations. We ran one-dimensional SNTHERM simulations at these 21 discrete locations (vertical profiles) at 12 cm intervals along the horizontal tree-to-tree transect axis from 01 March to 30 June, forcing the model with estimated sub-canopy meteorological conditions. As a result, we generated spatio-temporal matrices of snowpack conditions for each of the four canopy model scenarios, which varied as a function of canopy conditions and subsequent differences in simulated energy fluxes.

Stand scenario canopy parameters

We characterized living, red phase, grey phase and clearcut stand modelling scenarios using two stand parameters: canopy fraction (F_c) and effective leaf area index (LAI′). F_c is the relative fraction of obstructed sky and ranges between 0 and 1 (Hendrick *et al.*, 1971). LAI′ represents the total horizontal area of tree stems, needles and branches per unit area of ground ($m^2 m^{-2}$). Both F_c and LAI′ were estimated from hemispherical photographs of lodgepole pine canopies processed using Gap Light Analyzer software (Frazer *et al.*, 1999). On the basis of the photos from 16 stands in the Grand Lake area (CO, USA), Pugh and Small (2011, 2012) found approximate F_c values of 0.74 for both living and red phase stands and 0.66 for grey phase stands (lodgepole pine), which we used in this scenario analysis study. Pugh and Gordon (2012) estimated

Table I. Sensor description for flux tower at Niwot Ridge, Colorado.

Observation	Measurement height (m)	Instrument
Relative humidity (%)	2	HMP-35D, Vaisala, Inc.
Air temperature (°C)	2	HMP-35D, Vaisala, Inc.
Air temperature (°C)	8	HMP-35D, Vaisala, Inc.
Pressure (kPa)	12	PT101B, Vaisala, Inc.
Net radiation, $W m^{-2}$	25.5	CNR-1, Kipp & Zonen
Wind speed ($m s^{-1}$)	21.5	CSAT-3, Campbell Scientific

Note that this lists sensors used in this study; see Molotch *et al.* (2009) for a full description of the instrument cluster.

LAI′ values of 1.56, 1.35 and 1.09 in living, red phase and grey phase stands from hemispherical photography in 39 stands from across north–central Colorado (lodgepole pine dominant). These values were also used in this study to parameterize our modelling scenarios. For the clearcut stand, we assumed no presence of stems or canopies, and therefore, we set F_c and LAI′ to zero. Both F_c and LAI′ were used to estimate sub-canopy meteorological input provided to SNTHERM for the living, red phase and grey phase stand scenarios; above canopy meteorological values were used for the clearcut stand modelling scenario (i.e. F_c and LAI′ are equivalent to 0).

Model forcings

Shortwave radiation. Above canopy shortwave radiation ($\downarrow SW_a$) measured at the flux tower was adjusted to hourly sub-canopy shortwave radiation ($\downarrow SW_s$) as a function of canopy parameters using the approach of Hellström (2000). This approach effectively incorporated the Beer–Lambert law (Monsi and Saeki, 1953) into the canopy attenuation algorithm used by the Utah energy balance model (Tarboton and Luce, 1996):

$$\downarrow SW_s = \ \downarrow SW_a \exp(-a_v \text{LAI}) \qquad (1.1)$$

where a_v is the solar radiation extinction coefficient derived using spherical leaf angle distribution (Hellström, 2000):

$$a_v = 1/(2\cos Z), \qquad (1.2)$$

where Z is the solar zenith angle (Campbell and Norman, 1989). This approach explicitly resolves solar radiation attenuation by the canopy and also accounts for changing Z throughout the snowmelt season.

Snow surface albedo. The albedo algorithm used in SNTHERM accounts for grain growth, sun angle and cloud cover but requires a maximum snow albedo value. Snow surface albedo in a forested stand is affected by both snow age and litter deposition (Hardy *et al.*, 2000). For this simplified modelling experiment, we alter the maximum snow albedo value for each scenario on the basis of previous studies of litterfall and snow albedo relationships in beetle affected stands.

Snow surface albedo is dramatically impacted by tree death, including mortality related to beetle infestation (Boon, 2009; Winkler *et al.*, 2010). As a tree progresses through mortality, it loses much of its canopy as needles are deposited as litter at the forest floor; this process is particularly pronounced during the transition between the red and grey phases. During snow-covered periods, this litter deposition reduces snow surface albedo. Litter factor is the percent litter cover (L) normalized by stand basal area. Using litter factor values found by Pugh and Small (2011), we estimate percent litter cover (L) values of 4%, 7% and 2% for living, red phase and grey phase stands, respectively. We assumed zero litter input to the clearcut. We used the albedo reduction function of Pugh and Small (2011) to estimate maximum initial albedo at various levels of litter input, such that

$$\alpha_{+L} = -0.013L + \alpha \qquad (2)$$

where α_{+L} is the surface albedo and α is the albedo of a non-littered surface. It is important to note that snowfall input resets albedo to the value derived from Equation 2. Following this time step, changes in albedo are approximated by SNTHERM. Although it is likely that litter cover varies with distance from tree, we apply these average stand-scale litter values to all locations along the transect.

Longwave radiation. Sub-canopy incident longwave radiation ($\downarrow L_s$) was estimated using the approach of Hellström (2000):

$$\downarrow L_s = \ \sigma T_a^4 (1 - \text{SVF}) + \downarrow L_a \text{SVF} \qquad (3)$$

where σ is the Stefan–Boltzmann constant ($5.67 \times 10^{-8} \, \text{W m}^{-2} \, \text{K}^{-4}$), T_a is the air temperature in the canopy space (K) (measured at 8 m from ground at the flux tower), SVF is the hemispheric sky view factor (between 0 and 1), and $\downarrow L_a$ is the above canopy longwave irradiance (measured at 21.5 m from ground at the flux tower) (W m^{-2}). SVF was obtained using the approach of Metcalfe and Buttle (1998):

$$\text{SVF} = 41.1(\ln(100 - 100 F_c)) - 84.1 \qquad (4)$$

This resulted in SVF values of 0.51, 0.51 and 0.62 for the living, red phase and grey phase stand scenarios, respectively.

Wind speed. Sub-canopy wind speed, U_s (m s^{-1}), was estimated following the methods of Tarboton and Luce (1996):

$$U_s = \ (1 - 0.8 F_c) U_a \qquad (5)$$

where U_a (m s^{-1}) is the measured above canopy wind speed.

Precipitation. To determine spatially distributed estimates of precipitation along the tree-to-tree transect, we developed a simple linear regression model for snow interception at the tree well scale by using data collected by snow depth sensors placed at under, edge and open canopy positions in a living conifer stand (see *Field Methods*). To obtain tree well scale estimates of interception in the red and grey phase stand scenarios, we used percent differences in stand-scale interception between the living, red phase and grey phase scenarios. The resulting estimates of spatially distributed snow interception were used to approximate incident snowfall along the tree-to-tree transect for each modelling scenario. We initialized the model on 01 March and focused our analyses on ablation processes rather than those associated with accumulation. Hence, the details of our procedures for estimated precipitation are described in Appendix A.

RESULTS

Model forcings

Our modelling period extended from 1 March to 30 June, 2006. The average relative humidity was 63%, and sub-canopy

air temperatures generally oscillated near 0 °C, with consistent below zero temperatures in late-March (Figure 3). Most precipitation events were small in magnitude and occurred during mid-March and mid-April. Above canopy wind speed data were collected as 30-min averages and exhibited a maximum of $17 \, \text{m s}^{-1}$ and an average of $4 \, \text{m s}^{-1}$ for the modelling period. The daytime average above canopy shortwave irradiance was $530 \, \text{W m}^{-2}$.

The estimated fraction of shortwave radiation attenuated by the canopy (for the living, red phase and grey phase scenarios) decreased over the modelling period because of the declining solar zenith angle (Figure 4). In March, the theoretical canopies attenuated (on average) 66%, 60% and 52% of above canopy shortwave radiation for the living, red phase and grey phase modelling scenarios, respectively. By the end of May, estimated canopy attenuation was 56%, 51% and 44% of above canopy shortwave radiation for the living, red phase and grey phase modelling scenarios, respectively. Using 0.78 for α, we estimate maximum albedo values of approximately 0.72, 0.68, 0.75 and 0.78 for the living, red phase, grey phase and clearcut scenarios, respectively. These values were used to initialize albedo in SNTHERM.

The average above canopy longwave irradiance was $245 \, \text{W m}^{-2}$. Periods of low shortwave irradiance were generally coupled with periods of high longwave irradiance, assumed to be influenced by cloud cover. On average, longwave radiation was 18% and 14% higher in the living/red phase and grey phase scenarios, respectively, versus the clearcut scenario (i.e. above canopy measured longwave irradiance) (Figure 4). However, estimated sub-canopy longwave irradiance was as much as 47% greater in the living and red phase stands than the clearcut stand and as much as 37% greater in the grey phase stand than the

clearcut scenario. The greatest differences in estimated longwave irradiance between the forested scenarios (i.e. living, red phase and grey phase) and clearcut scenario occurred at midday. Estimated sub-canopy wind speeds were reduced from above canopy values by 59% for both the living and red phase scenarios, and by 53% for the grey phase scenario, and were treated as above canopy for the clearcut scenario (Figure 4).

Initial conditions

Data from the tree-to-tree trench were used to initialize SNTHERM. Snow depth increased with distance from tree, such that a maximum depth of 72 cm was found at the centre of the trench where canopy interception is minimized (Figure 5). A common vertical snow temperature profile was observed across the snow trench, with a snow surface temperature around −2 °C, decreasing within the first 10 cm to cooler temperatures of approximately −4 °C and then increasing toward the snow–ground interface to approximately −2 °C. Similarly, a common snow density structure was observed, with lower densities near the snow surface and at the base of the snowpack and higher densities in the middle of the snowpack. The average density on 28 February was $250 \, \text{kg m}^{-3}$ and ranged between 208 and $282 \, \text{kg m}^{-3}$. Despite some similarities in the trends exhibited by snow temperature and density profiles, snow depth was the most prominent snowpack characteristic that varied between the under (i.e. 25 cm from tree bole) and the edge and open canopy locations (i.e. 75 cm from tree bole and at the trench centre). Grain sizes measured on 28 February (Figure 6(A)) generally increased with depth and proximity to the transect centre, with facets found from the base of the snowpack to
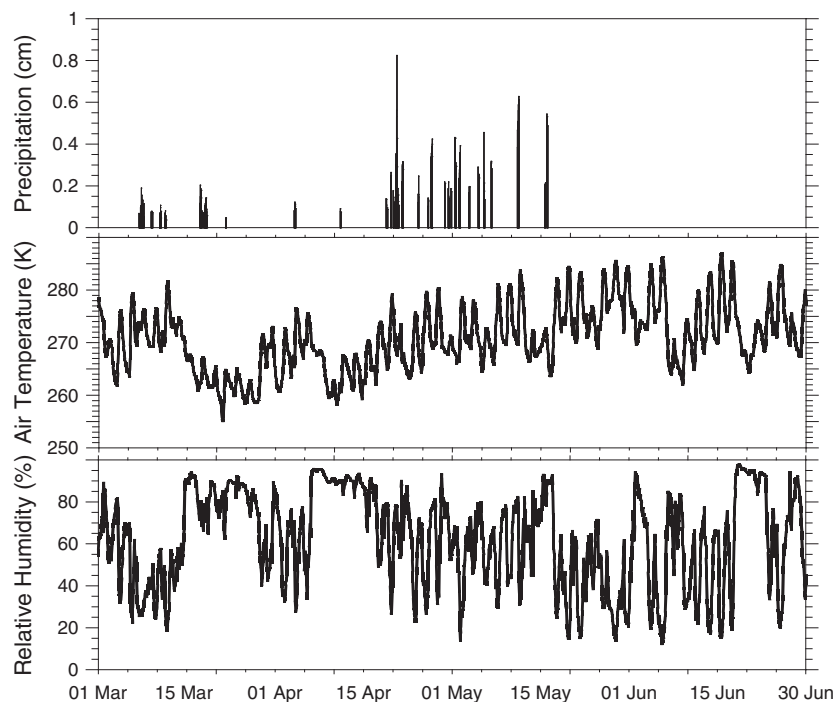

Figure 3. Precipitation estimated from the 'open' depth sensor for the modelling period, and air temperature and relative humidity measured at the flux tower.
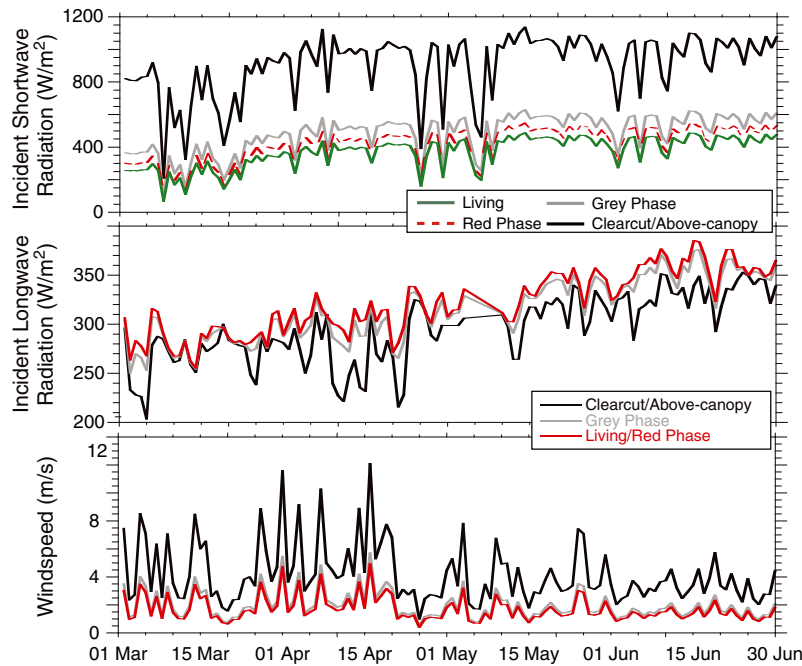
Figure 4. Modelled daily average sub-canopy wind speed, daily maximum shortwave radiation and daily maximum longwave radiation for living, red phase, grey phase and clearcut stand scenarios for the modelling period. It should be noted that the estimated values given to SNTHERM are at a 30-min temporal resolution.
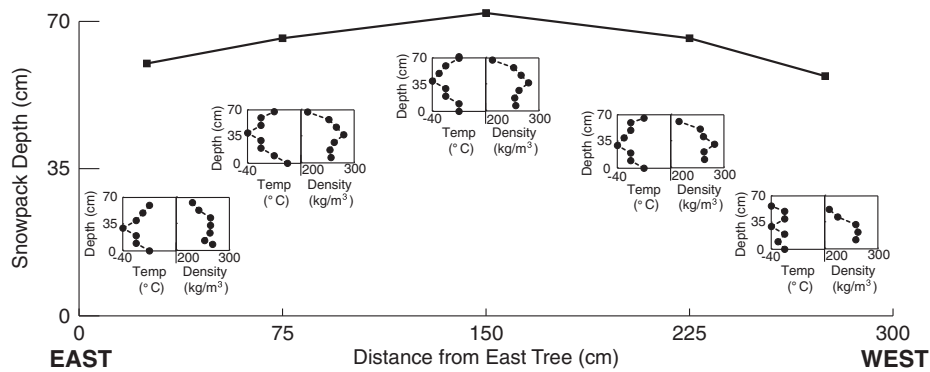

Figure 5. Profiles of snow temperature and density data collected along the east–west snow trench on 28 February 2006.

approximately 7 cm from the snow–atmosphere interface at all locations along the transect.

Spectrally derived OGR values (from spectroscopy) ranged from 0.03 to 0.142 mm. As discussed previously, relationships between OGR and GGR were established to extrapolate GGR to the OGR sampling resolution. OGR data and grain sizes measured by a hand lens (GGR) in February and March yielded the best-fit model,

$$\text{GGR} = 127949 \times \text{OGR}^{1.964} \qquad (6)$$

with an r^2 value of 0.72 and a p-value of 0.01 (Figure 6(B)), where GGR and OGR values are in m. We adjusted our OGR measurements by this relationship to obtain GGR values for model input, which allowed for a higher level of detail than the hand lens measurements.

Model performance

We compared the previously described *in situ* measurements made in the living stand to the modelled results to assess SNTHERM's performance in the living scenario. The snow depth sensors placed at the under and open canopy locations measured average snow disappearance dates on 15 May and 25 May, respectively (Figure 7(A)). The model results for the living scenario exhibited snow disappearance dates of 25 May and 05 June for the under and open canopy locations, respectively. Hence, the difference between modelled under versus open snow disappearance timing in the living scenario was consistent with the measured difference in snow disappearance timing. However, SNTHERM over-estimated the duration of snow persistence by 10 days. We also found that on average there was a 25 cm difference in modelled snow depths at the open and under canopy position for the living scenario results that is consistent with measured differences between open and under canopy positions. However, maximum modelled snow depths were approximately 60% and 50% of the maximum measured snow depths (from the snow depth sensors) for the open and under canopy locations, respectively (Figure 7(A)). SNTHERM
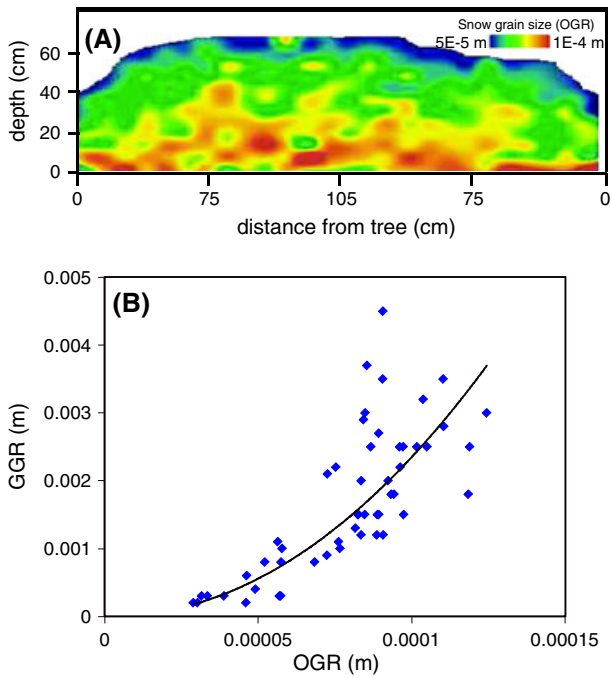
Figure 6. (A) Grain size distribution (optical grain radius (OGR)) for the February snowpack. (B) Model of best-fit for OGR versus geometric grain radius (GGR), r^2 value of 0.72 and $p < 0.01$.

underestimated the snow water equivalent (SWE) measured at the snow trench during March (accumulation season) by 11 cm but did relatively well predicting SWE in April and May (less than 1 cm error) (Figure 7(B)). SNTHERM did

relatively well predicting the vertical distribution of snow grain size, particularly in March and April (Figure 7(C)). Measurements made with a hand lens exhibited a greater range in snow grain size that was not captured with the spectroscopy measurements used to initialize the model. As a result, the modelled vertical distribution of grain size was more similar to measurements made by the spectrometer than those made with a hand lens. The average measured snow trench measurements on 24 March, 19 April and 16 May were $-2\,°C$, $-0.9\,°C$ and $0\,°C$, respectively. The average modelled snow temperatures in the living modelling scenario for these dates were similar to those observed, with values of $-1.62\,°C$, $-1.09\,°C$ and $0\,°C$ for 24 March, 19 April and 16 May, respectively.

Although the model results were mixed in terms of overall accuracy, our focus is on the relative differences in snowpack conditions under the different scenarios. Furthermore, the model showed adequate performance with respect to SWE, which is the most hydrologically relevant variable of all the comparisons. The degree to which model accuracy affects snowpack differences between scenarios is considered in the Discussion section.

Modelled snowpack properties

We found increasing homogeneity in the spatial distribution of snowpack properties with canopy loss and with the onset of melt. During pre-melt conditions (e.g. 21 March), the modelled snowpacks for all scenarios displayed distinct
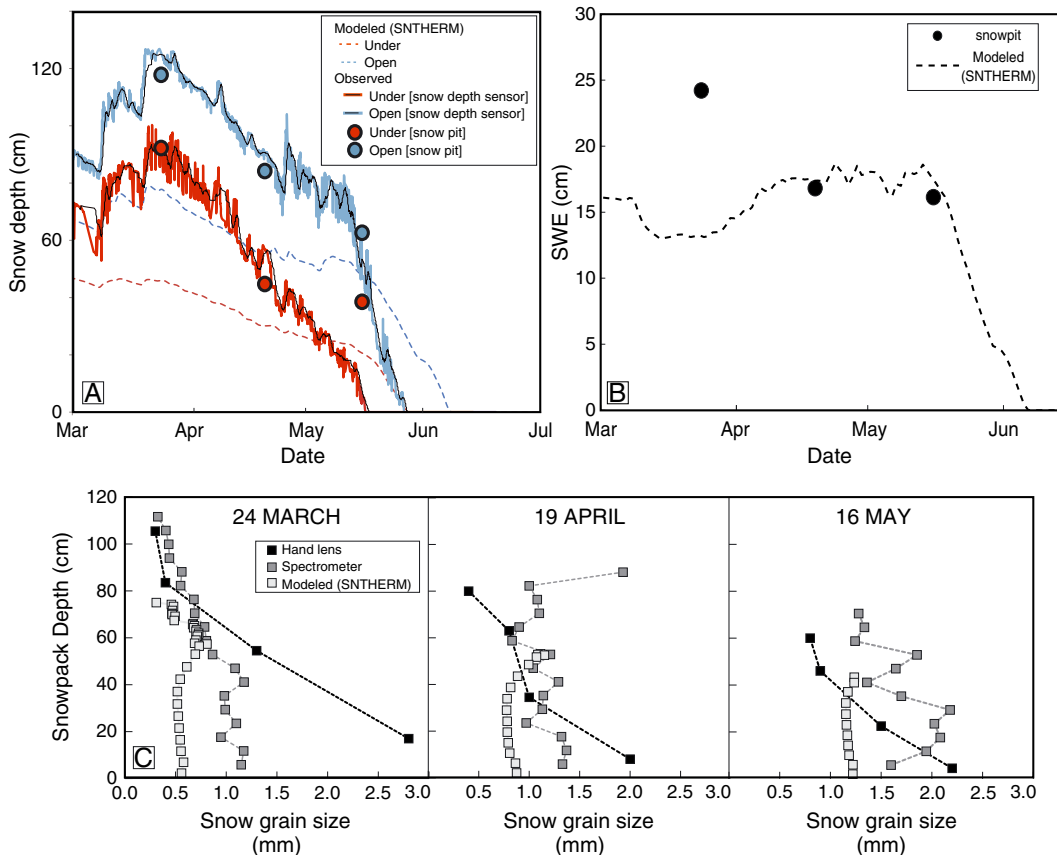

Figure 7. (A) Observed and modelled snow depths at the under and edge canopy locations. (B) Observed and modelled snow density. (C) Observed (from spectroscopy) and modelled snow grain sizes for the tree-to-tree transect on 24 March, 19 April and 16 May 2006.

upper, middle and basal layers, as shown by the vertical profiles of snow temperature, density and grain size (Figure 8), which were designated from general trends in the profiles of snow characteristics (i.e. wherever there was a sudden change from high to low values or vice versa). It should be noted that every data point output from SNTHERM (Figure 8) is a layer that was generated by SNTHERM; we group layers with similar characteristics into this more general three-layer scheme for analytical purposes. The general simulated snow temperature profile for all modelling scenarios and all canopy positions (Figure 8, left column panels) exhibits increasing temperature with depth for the upper layer, decreasing snow temperature with depth for the middle layer and again increasing snow temperature with depth for the basal layer. When comparing the under canopy and open locations along the transect, the greatest spatial heterogeneity in snowpack temperature occurred under the red phase scenario (Figure 8, left column, second panel from top). The modelled temperatures of the upper and middle layers in the red phase stand were 19% and 22% colder (respectively) at the under canopy positions versus the open canopy positions. The greatest differences in modelled snowpack temperature between the edge and open canopy positions occurred in the basal layer (below 50 cm depth) for the living, red phase and grey phase canopy positions; there was no difference in snowpack temperature for layers at the under and edge canopy positions in the clearcut scenario. The living scenario snowpack also exhibited spatial heterogeneity in snowpack temperature (Figure 8, left column, top panel), with average temperature values diminished by 10% from the open to under canopy positions for both the upper and middle layers. The grey phase and clearcut modelled

snowpacks exhibited less spatial heterogeneity in snow temperature across the tree-to-tree transect for the upper and middle layers versus the living and red phase scenarios. In all scenarios except the clearcut, the snowpack temperature was warmest for the basal layer (by more than one degree) for all canopy positions. In contrast, the average temperature for the basal layer in the clearcut was colder than the middle or upper layer at all positions (by less than 1°). In general, the upper layers (for all canopy positions) exhibited the coldest average temperatures in the living phase scenario and the warmest average temperatures in the clearcut stand.

Differences in snow density with depth and tree-to-tree canopy position within each modelling scenario (Figure 8, middle column) were similar to the differences in snow temperature. In general, modelled snow density was lowest for the upper and middle layers, with a distinct increase in density at the middle–basal layer interface. There was a greater difference in snow density between the under and open positions than the edge and open positions. Densities were on average only slightly higher for the under and edge canopy locations than the open canopy locations for all modelled snowpack layers and all modelling scenarios. The living stand exhibited the greatest differences in average density for the middle layer of the snowpack (20% greater at the edge position than the open position and 76% greater at the under position than the open position) (Figure 8, middle column, top panel). The average snowpack densities for the middle layer became more similar with the progression of tree mortality, with densities 71% and 48% greater at the under location versus the open location for the red phase and grey phase scenarios, respectively. There was almost no difference in average layer density between all positions in the clearcut scenario (Figure 8, middle column, bottom panel). The lower density snow for the upper and middle layers is a result of the most recent precipitation event and associated low density of new snowfall.

Finally, the modelled grain size profiles for each scenario were coupled closely with both the temperature and density profiles; the smallest grain sizes were simulated in the upper layer of the snowpack (i.e. cold, low density new snow) with larger grains at the middle and basal layers (Figure 8, right column). The greatest differences in grain size between canopy locations occurred for the upper layer in all model scenarios except the clearcut scenario, for which there was very little variability in grain size between the upper, middle and basal layers. Like density, the greatest difference in snow grain size for the upper layer occurred for the green phase scenario, in which the average grain size was 76% greater at the under position than the open position (Figure 8, right column, top panel). This increase in grain size between the under and open canopy positions was diminished to 71% in the red phase scenario and 53% for the grey phase scenario, exhibiting a spatial homogenization of grain size with the progression of tree mortality.

At a date characteristic of the melt period (e.g. 10 May), the modelled snowpacks exhibit homogenous distributions of snow densities and grain sizes (i.e. >5% difference in modelled snow properties between canopy positions) and
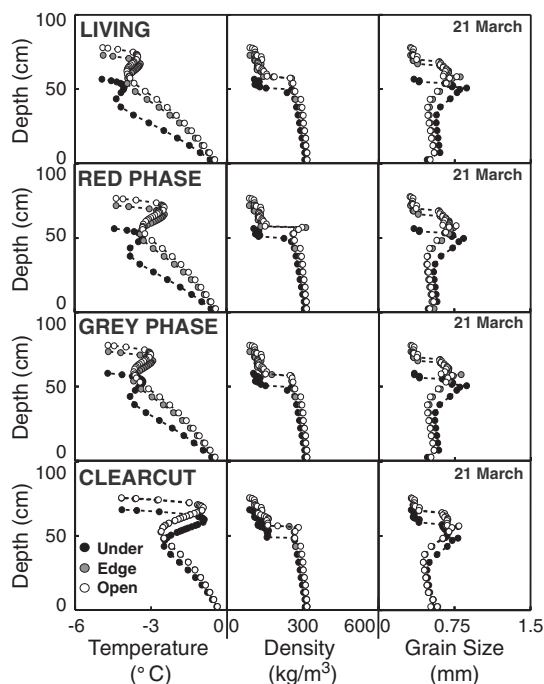

Figure 8. Profiles of snowpack characteristics at 'under', 'edge' and 'open' canopy positions for living, red phase, grey phase and clearcut modelling scenarios for a timestep during the pre-melt season (21 March).

isothermal temperature at 0 °C (Figure 9). The average densities and grain sizes of the snowpacks were significantly greater during the melt period than the pre-melt period (i.e. p < 0.05) within each modelling scenario. Depth was the least variable across the tree-to-tree transect for the clearcut modelling scenarios.

Modelled snowmelt

The snowpack in the clearcut scenario became and remained isothermal at 0 °C 10 days earlier than the other three modelling scenarios (Figure 10). The red phase scenario was isothermal for a longer period than the living or grey phase scenarios. Model estimates of snowpack temperature became isothermal at 0 °C during four periods in the living, red phase and grey phase scenarios and three periods in the clearcut scenario (Figure 10). The living and grey phase scenarios exhibited identical trends in the timing of isothermal conditions. Whereas the red phase scenario snowpack first became isothermal on the same date as the clearcut scenario, the date that it became and remained isothermal was similar for the living and grey phase scenarios. The first isothermal period occurred from 9 April to 18 April in the red phase and clearcut scenarios and from 13 April to 18 April in the living and grey phase scenarios. The second isothermal period occurred at the same time in all scenarios (22 April to 25 April). The third isothermal period occurred from 27 April to 4 May in the living, red phase and grey phase scenarios. The clearcut

scenario also became isothermal on 27 April but remained isothermal for the remainder of the modelling period. The living, red phase and grey phase scenarios became permanently isothermal on 7 May.

In the living scenario, model results show that snow first disappeared from the tree-to-tree transect on 25 May, and all snow disappeared by 5 June (snow disappearance occurred over 11 days). The grey phase scenario exhibited a similar timing of snow disappearance, with snow first melting out from the model transect on 26 May and finally completely disappearing on 5 June. The clearcut scenario melted out 11 days earlier than the living scenario and exhibited the least variable timing of snow disappearance (22 May to 25 May, 3-day range in snow disappearance) (Figure 10, red and blue lines). The red phase scenario snowpack disappearance date was earlier than both the living and grey phase scenarios by four days but exhibited a similar range in the timing of melt out along the transect (21 May–31 May, 10 days).

The maximum modelled SWE for the modelling period was highest in the grey phase scenario (21.9 cm) (Table II). The average tree-to-tree transect SWE for the modelling period was lowest for the red phase and clearcut scenarios (10.2 cm) and highest for the grey phase scenario (11.3 cm). We expected that a loss of canopy would result
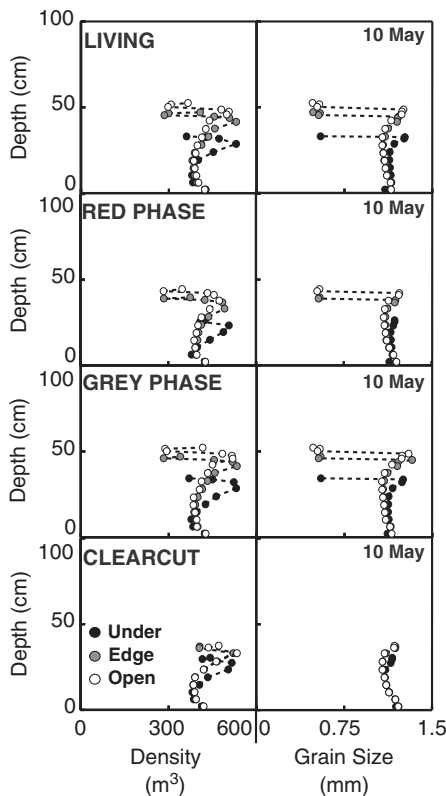
Figure 9. Profiles of snowpack characteristics at 'under', 'edge' and 'open' canopy positions for living, red phase, grey phase and clearcut modelling scenarios for a timestep during the melt season (10 May). Snow temperature profiles are not shown as all snow temperatures were isothermal at 0 °C.
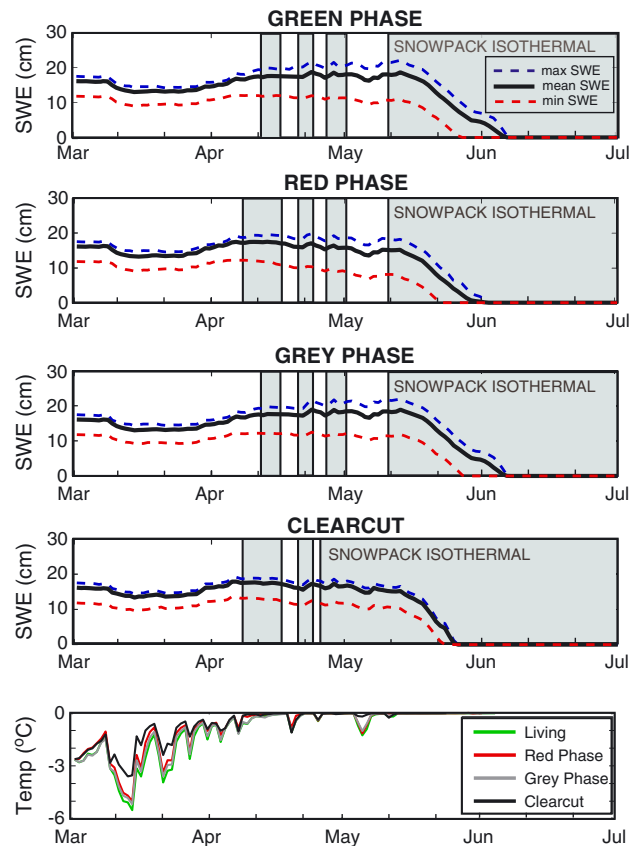
Figure 10. Modelled snow water equivalent (SWE) for living, red phase, grey phase and clearcut stand scenarios integrated over the tree-to-tree transect for the ablation season. Grey shading indicates when the entire modelled snowpack along the tree-to-tree transect is isothermal at 0 °C. Average snowpack temperature for each modelling scenario is shown in the bottom plot.

Table II. Modelled snow water equivalent summary statistics for the modelling period.

SWE	Living	Red phase	Grey phase	Clearcut
Maximum (cm)	22.1	19.7	21.9	19.1
Mean (cm)	11.2	10.2	11.3	10.1
Average coefficient of variance	0.2	0.2	0.2	0.1

in a reduced effect of distance from tree on snowpack processes and that this would be reflected in less variability along the tree-to-tree transect. The clearcut scenario exhibited half the variability in the spatial distribution of SWE at the tree well scale of the living, red phase, or grey phase modelling scenarios, with average coefficient of variation values of 0.1 and 0.2, respectively. Finally, the melt rate during the last isothermal period was highest for the red phase scenario (0.71 cm day^{-1}) and lowest for the clearcut scenario (0.60 cm day^{-1}). Melt was slower in both the living scenario (0.66 cm day^{-1}) and in the grey phase scenario (0.68 cm day^{-1}) compared with the red phase scenario.

DISCUSSION

Although a comparison of measurements made in the living stand at Niwot Ridge and model results from the living stand scenario showed that SNTHERM predicted SWE relatively well during the melt season, we also found an unde-restimation of maximum SWE accumulation and an over-estimation of the dates of peak SWE and snowpack disappearance. Although we estimated precipitation inputs to SNTHERM from the snow depth sensors (see Appendix A), we were unable to capture the magnitude of snowfall events in SNTHERM, particularly the largest snowfall events in mid-March and late-March. It is likely that some of the error associated with our underestimation of precipitation may be from our derivation of the forcing precipitation, which was computed using measured depths and the Alta function to predict the density of new snow. Potential errors associated with the Alta function (Fassnacht and Soulis, 2002) and with the snow depth sensors may have resulted in this large underestimation of precipitation. It is also possible that SNTHERM over-estimated the settling rate (i.e. compaction) of new snow (Coléou et al., 2004). Additionally, model uncertainty may be attributed to the differences between the actual site canopy structure and the canopy structure parameters used to adjust above canopy meteorological forcing data to the sub-canopy surface. Because the canopy parameters in our model were not derived from Niwot Ridge, it is unlikely that our adjusted sub-canopy meteorological forcings were representative of the actual sub-canopy site meteorology at Niwot Ridge. Furthermore, we anticipate that some of the differences between our modelled results and observations at Niwot Ridge may be related to how we adjusted energy balance forcings for the sub-canopy environment. For example, we did not alter radiation as a function of distance from trees, although the effects of canopy on radiation are highly variable in both space and time (Hardy et al., 2004; Musselman et al., 2012). The results from our clearcut scenario (i.e. no alteration of above canopy meteorological data) exhibit the same snow disappearance date as measured by the open depth sensor (25 May), suggesting that our general stand-scale canopy model over-estimated canopy attenuation of shortwave radiation particularly in forest clearings, resulting in an underestimation of energy incident to the snowpack and snowmelt rates.

Snowmelt models tend to exhibit greater errors in forested sites than open sites because of micro-scale processes related to sub-canopy meteorology (Rutter et al., 2009). Errors in snow disappearance dates from our study (i.e. 10 days on average) were similar to those exhibited by other studies in forested areas (as much as approximately 1 month under-estimation or over-estimation of snow disappearance date) (e.g. Link and Marks, 1999; Frankenstein et al., 2008; Rutter et al., 2009; Ge and Gong, 2010; Musselman et al., 2012). Furthermore, the modelled tree well scale spatial variability and distribution of snow properties (i.e. density and snow grain size) were similar to observations made in monthly snowpits. Although the absolute model error with respect to living stand snow depth was considerable, modelled differences between open and under canopy locations were quite accurate. Thus, the model performance was deemed adequate to compare relative differences between model scenarios (living, red phase, grey phase and clearcut) at the tree well scale.

We anticipate that there were certain additional errors in our representation of canopy structure-related impacts on sub-canopy energetics. The Beer–Lambert law (Monsi and Saeki, 1953) used by the Utah energy balance model (Tarboton and Luce, 1996; Hellström 2000) was developed in a deciduous stand (Hirose, 2005) and may over-estimate the attenuation of solar radiation in the canopy compared with a needle-leaf canopy (Sicart et al., 2004; Liston and Elder, 2006). Furthermore, this shortwave radiation model does not account for sub-canopy light scattering and instead simply reduces the amount of incident above canopy solar radiation as a function of the solar zenith angle and LAI$'$. We expect that this may have generated the most error for the living and red phase scenarios, where light scattering would occur off of needles as well as tree stems. Our approach for estimating sub-canopy longwave radiation is also subject to error, as the SVF value used in the longwave radiation model was estimated using an empirical model by Metcalfe and Buttle (1998) from data collected in a forest composed primarily of black spruce, which has different needle orientation and canopy composition than lodgepole pine forests. Also, this longwave radiation model does not account for longwave emission by tree stems and may have resulted in an underestimation of sub-canopy longwave radiation. The errors associated with longwave radiation modelling likely had the largest effect in the red phase stand but is complicated by the partitioning of longwave radiation emission from the canopy and the tree stems (discussed in further detail in the following text). The combination of these potential underestimations of

sub-canopy radiation values could have resulted in the greatest underestimation in snowmelt rates and snow disappearance timing for the living and red phases of tree death, where we estimated the greatest reductions in sub-canopy radiation. Furthermore, it is likely that the actual differences in snowmelt rates and timing between different phases of MPB-associated tree death may be greater than our model results suggest.

Nevertheless, results from these scenario analyses indicate changing snowpack melt dynamics with the progression of tree death and removal. The living and red phase scenario snowpacks became permanently isothermal on the same date, but the red phase scenario exhibited complete snow disappearance 4 days earlier than the living scenario. This is relatively consistent with results from field studies by Pugh and Small (2011), who measured no difference in the date that a snowpack became isothermal between living and red phase stands and up to a week earlier snow depletion date for red phase stands. Pugh and Small (2011) also found that snow ablation rates were greater in the red phase stands than the living stands. We found similar results in our modelling study: the melt rate in the red phase stand was higher in the red phase scenario compared with the living scenario during the primary ablation period (the last isothermal period). Pugh and Small (2011) observed that there was increased snowmelt in red phase stands coincident with the emergence of a litter layer at the snow surface, after the snowpack became isothermal. To assess whether our modelled change in snow disappearance timing was solely the result of the change in albedo between the living and red phase scenarios, we ran the living scenario in SNTHERM but applied the red phase scenario albedo value instead of the living scenario albedo value. Snow disappearance along the tree-to-tree transect for this albedo test scenario occurred from 23 May to 3 June, which was 2 days earlier than the living scenario results. If the differences in albedo were the only reason for earlier snow disappearance in the red phase scenario compared with the living scenario, we would have found a 4-day difference in snow disappearance between the albedo test scenario and living scenario. Still, half of the difference in the timing of snow disappearance between the living and red phase scenarios was from the change in albedo alone.

Our simplified change in albedo from the living to red phase scenarios may have underestimated the actual difference in litter cover and snow surface albedo between and within living and red phase stands because we applied average stand-scale values from Pugh and Small (2011). The method used by this study for the treatment of albedo only approximates the relative differences in albedo during the modelling period and likely under-estimates the absolute effects of litter on snow surface albedo over the course of the ablation season (Hardy *et al.*, 2000; Melloh *et al.*, 2002; Pugh and Small, 2011). However, we expect the relative differences in albedo values between scenarios to be generally correct in sign. Our approach does not account for the increasing effect of litter on snow albedo with the progression of the ablation season due to the reemergence of litter layers at the surface of the snowpack (Winkler *et al.*, 2010) and also does not account for the combination of litter layers within the snowpack. More detailed representation of litter impacts on snow albedo are needed to improve the accuracy of these predictions. Hardy *et al.* (2000) applied a more detailed litter process algorithm in SNTHERM, but this version of SNTHERM has yet to be publicly released. Future ecohydrologic studies should address these complex litter and snow albedo processes by making detailed observations of needle layer dynamics in seasonal snowpacks in different phases of MPB-affected stands and should then work toward developing an improved albedo algorithm to be incorporated into spatially distributed snowmelt models.

An increase in shortwave transmission with the progression of canopy loss would make snow surface albedo a more important variable in snow melt processes (Sicart *et al.*, 2004; Winkler *et al.*, 2010). Temporal changes in litter-drop rates coinciding with increasing shortwave radiation should be factored into future modelling studies, as it is likely that snow surface albedo plays a dominant role in the snowpack energy balance with increase sky view associated with tree death (Hardy *et al.*, 1997; Link and Marks, 1999; Melloh *et al.*, 2002; Sicart *et al.*, 2004). Additionally, aspect and slope were not considered in this study given that the study site was relatively flat. Future efforts should explore the importance of slope and aspect and associated variability in the distribution of shortwave radiation and the relative differences in ablation rates between stands in different phases of mortality (Winkler *et al.*, 2005).

Modelled snowpack temperature and snow disappearance dates were extremely similar for the living and grey phase scenarios. This is consistent with Boon (2009), which also reported the same timing of snow disappearance in a living and dead stands at a site in BC in 2008; in 2007 in BC, the snow disappeared from the dead stand 4 days earlier than the living stand. The meteorology at the BC site in 2008 was characterized by alternating periods of ablation and accumulation, which is more similar to the meteorology at Niwot Ridge in 2006 used to force SNTHERM. Our modelled results show very little difference between living and grey phase scenario melt rates. This is consistent with the comparative observations in living and red/grey phase transition stands by Pugh and Small (2011) but dissimilar to their findings in grey phase stands, which showed grey phase stand melt rates two times greater than that of living stands. We hypothesize that these differences between our modelling results and the observations of Pugh and Small (2011) could be the result of (1) different meteorology at each site and for each year (i.e. 2006 versus 2010), (2) differences in our modelled and actual interception in living, red phase and grey phase stands (Pugh and Small, 2012) and (3) differences in the stand scenario canopy parameters we used for this modelling scenario analysis and the actual canopies present at Pugh and Small (2011) study sites.

We modelled a snow depletion date 11 days earlier for the clearcut scenario than the living stand. This is consistent with

observed differences in snow disappearance dates between living and clearcut stands (3–11 days) (Winkler *et al.*, 2005; Boon, 2009). However, the modelled clearcut snowpack exhibits a slow ablation rate for much of the time that the modelled snowpack is isothermal, followed by a period of rapid SWE depletion (i.e. melt) resulting in snow disappearance over the course of approximately 1 week. This is likely a result of the meteorology inputs provided to the model; this period of rapid melt and the 2 days preceding it were characterized by both warm day and nighttime temperatures (daytime temperatures reached maximum of approximately 20 °C, and nighttime air temperatures remained above 0 °C).

Results exhibited decreasing heterogeneity in the timing of snow disappearance along the tree-to-tree transect with the progression of tree death and tree removal. Initializing the model with a spatially heterogeneous snowpack for all four scenarios caused the 3-day range in snowmelt timing in the clearcut scenario. Previous research at the stand scale has shown that there is no significant difference in SWE accumulation in living and red phase stands but that snow accumulation may range from 11% to 74% greater in grey phase stands than living stands (Boon, 2009; Pugh and Small, 2011). We initialized SNTHERM with measured spatially distributed snow conditions to understand potential changes in this distribution with the progression of the ablation season and with the progression of tree death and canopy removal. For the purposes of this study, we are interested in the relative differences between model scenarios, rather than absolute magnitude of SWE, ablation and snow disappearance timing, or snowpack properties. Future studies should make spatially distributed measurements of snow properties at both the tree well and stand scales in red phase, grey phase and clearcut areas over multiple years for model calibration and validation.

Intra-stand variability in snow properties and the timing of isothermal conditions may also be driven by longwave irradiance from tree boles and not solely from the canopy (as we treated longwave radiation in this modelling study) (Sicart *et al.*, 2004). Pomeroy *et al.* (2009) found enhancement of longwave radiance from tree boles when exposed to direct shortwave radiation and hypothesized that greater amounts of longwave enhancement in stands may result from the loss of canopy and increase in the number of dead tree boles. Additionally, studies have shown that dead canopies emit less longwave radiation than live canopies (e.g. Boon, 2009). However, these factors were not considered here because of lack of data to drive more complex algorithms. We likely most greatly underestimated longwave radiation in the grey phase scenario, when there are no longwave emissions from the canopy (because of loss of canopy biomass) but there may be an enhancement of longwave radiation from tree boles (Pomeroy *et al.*, 2009). These processes may have a significant impact on the snowpack energy balance of MPB-affected stands and should be considered for future monitoring and modelling studies.

We found a decrease in the spatial heterogeneity of snowpack properties with the progression of canopy loss and melt. This heterogeneity was partially maintained in the grey phase scenario, suggesting that dead stands have notably different snow processes than clearcut areas. Thus, post-infestation forest management could greatly alter the hydrology of these stands. Spatial heterogeneity in snowpack temperature along the tree-to-tree transect within each model scenario was partially a function of the snowpack used to initialize the model, as well as differences in incident precipitation at each canopy position. All other forcing variables in the model (i.e. shortwave and longwave irradiance, wind speed and albedo) were averaged for the stand and thus identical for all canopy positions within each scenario. We estimated snow density (and thus SWE) to be greater at the open canopy position than at the under canopy position along the tree-to-tree transect, which is consistent with previous studies (Faria *et al.*, 2000; Fassnacht *et al.*, 2006; Musselman *et al.*, 2008). Further study including direct observations of energy fluxes in different canopy positions is needed (Hardy *et al.*, 1997; Link and Marks, 1999; Pomeroy *et al.*, 2009). Our stand-scale treatment of meteorological variables likely resulted in an underestimation of the differences between modelling scenarios with respect to the intra-stand distribution of snow properties and snowmelt timing.

Differences in the distribution of snowpack properties and the timing of melt with the progression of tree death have numerous implications for the hydrology and ecology of MPB-affected and managed stands. A greater range in the date of snow disappearance along the tree-to-tree transect signifies a longer period of stand-scale water availability in the soil. This may sustain transpiration rates and increase total vapour fluxes to the atmosphere (Tague, 2006; Molotch *et al.*, 2009). When canopy was removed (i.e. clearcut scenario), we estimated a considerable acceleration in the timing of snowmelt at the tree well scale. This more rapid loss of SWE from the snowpack may alter hydrologic pathways such that less water is available to vegetation (Tague, 2006). Studies have shown that snow depth, duration of snow cover and snowmelt rates control microbial activity (Brooks *et al.*, 1996, 1998; Monson *et al.*, 2006; Williams *et al.*, 2009); generally, the snowpack insulates the soil at the ground–air interface, allowing for relatively warm and stable soil temperatures and thus high rates of microbial activity. Hence, a uniform distribution of deeper snow under the clearcut scenario may increase respiration rates and enhance carbon efflux to the atmosphere. During spring, an accelerated and larger snowmelt pulse may result in rapid N export of microbially produced nitrate in soils, which has implications for ecologic health and stream chemistry.

The results of this study provide insight into the hydrologic implications of MPB mortality and associated forest management strategies. Removal of dead trees (i.e. salvage harvesting and clearcutting) may result in a greater magnitude of available SWE and greater energy available for snowmelt; however, if the higher melt flux is also associated with an earlier timing of snow disappearance, this could result in a longer snow-free period, earlier soil drying and a reduction in seasonal average soil moisture (McNamara *et al.*, 2005; Pugh and Gordon, 2012).

Conceptually, a decline in available soil moisture later in the growing season may actually impede forest regeneration (although this is also dependent on pre-existing stand conditions) compared with a red or grey phase stand, which also displayed higher amounts available SWE compared with the living phase but a slower melt pulse and longer duration of melt than a clearcut stand.

CONCLUSIONS

We presented a scenario analysis of snow ablation at the tree well scale in living, red phase, grey phase and clearcut stands by using the same initial snowpack and snowmelt forcing variables scaled for canopy parameters. We found the same timing of isothermal conditions and snow disappearance timing in living and grey phase stand scenarios; the red phase stand exhibited similar timing of isothermal conditions and duration of snowmelt, but all snow disappeared 4 days earlier than the living phase and grey phase scenarios. The clearcut scenario became isothermal 10 days earlier than the living, red phase and grey phase scenarios and exhibited complete snow disappearance 11 days earlier than the living scenario. The timing of snow disappearance along the tree-to-tree transect became less variable with increasing canopy loss. Snowpack properties became more homogenous with canopy loss and the onset of snowmelt. Red and grey phase scenarios still exhibited a tree well signature in terms of the distribution of snow depth and snow properties along the tree-to-tree transect, and it was only in the clearcut scenario that there was a considerable spatio-temporal homogenization of snow depth, properties and melt. The micro-scale homogenization of snow processes with canopy reduction may lead to a decline in available soil moisture and corresponding increase in vegetation stress. This could have important effects on nutrient cycling, hydrologic flowpaths and stand regeneration, and thus, these results may help inform forest management strategies with respect to water resources and ecosystem services.

APPENDIX A

We used snow depth data collected by the spatially distributed snow depth sensors for 1 March–30 June to develop the tree well scale interception model for the living stand. Using averages of the 'under', 'edge' and 'open' depth sensors, we first removed noise from the collected data by using a 6-h central moving average. Next, we computed the change in depth for each hourly timestep. An increase in snow depth (S, cm) was assumed to be snowfall that is accumulating on the ground surface. Erroneously

small values (i.e. >0.5 cm) were removed from the dataset. For a simplified empirical model, we assumed that an increase in depth at an open sensor location (S_o) was representative of 100% of the above canopy snowfall amount and 0% canopy interception, and the increases in depths at the canopy under and edge sensor locations (S_u, S_e) were some fraction of the total snowfall because of some amount of canopy interception.

We found that the under and edge sensor (approximately 0.9 and 1.3 m from tree boles, respectively) on average received 39.7% and 19.6% less snowfall per event than the open sensors (approximately 1.7 m from tree bole). From this, we approximated interception as a function of proximity from tree bole:

$$i_{living,x} = 0.8986 - 0.5373x \qquad (7a)$$

where $i_{living,x}$ is the living stand interception (between 0 and 1) as a function of distance from tree bole (x, m).

To find estimates of interception as a function of distance from tree bole for the red and grey phase scenarios, we scaled our living stand interception model (Equation (7a)) by percent differences in average stand-scale interception between the living and red or grey phase scenarios. In this regard, we used the stand-scale interception model of Pomeroy *et al.* (2002):

$$i_{stand} = 3.94 \times LAI' \left(1 - e^{\frac{-F_c \times S}{5.8 LAI'}}\right) \qquad (7b)$$

where i_{stand} is the stand-scale snowfall interception (cm). We calculated i_{stand} for all time steps during the modelling period for values of F_c and LAI' of the theoretical living, red phase and grey phase scenarios. We found the average stand-level interception rates for these three scenarios by

$$\bar{i}_{stand} = \frac{1}{n} \sum_{j=1}^{n} \frac{i_{(j)}}{S_j} \times 100 \qquad (7c)$$

where i_{stand} is the average stand-level interception (%), n is the total number of time steps, i_j is the amount of snowfall intercepted at a given timestep j and S_j is the above canopy snowfall amount. From estimated i_{stand} for the living, red phase and grey phase stand scenarios, we found that the living stand would intercept 41.58% of the total snowfall, the red phase stand would intercept 40.49% of the total snowfall and the grey phase stand would intercept 35.38% of the total snowfall. Therefore we estimated that i_{red} and i_{grey} were approximately 97% and 85% of $I_{avg(living)}$, respectively. The Pomeroy model may over-predict actual interception for grey phase stand conditions (Pugh and Small, 2012) but is likely correct in sign for the relative change in interception associated with diminished canopy.

We applied these percent differences as scaling coefficients to Equation (7a) to obtain tree well scale models for estimating interception as a function of distance from tree bole for the red and grey phase stand scenarios:

$$i_{red} = 0.8717 - 0.5212x \qquad (7d)$$

$$i_{grey} = 0.7818 - 0.4675x \qquad (7e)$$

We then apply these models to our total incident snowfall values derived from the open snow depth sensors to obtain spatially distributed estimates of snowfall S (i.e. snowfall for each of the 21 SNTHERM modelling profiles) for living, red phase and grey phase stand modelling scenarios.

Finally, SNTHERM requires forcing with precipitation, not snowfall depth, and thus snowfall values were converted to equivalent depths of liquid water by using the Alta function to estimate new snowfall density (on the basis of data by LaChapelle, 1969) (Anderson, 1976):

$$\rho_{ns(t)} = 0.05 + 0.0017\big(T_{w(t)} - 258.16\big)^{3/2} \qquad (8)$$

where $\rho_{ns(t)}$ is the density of new snow (kg m^{-3}) at time t and $T_{w(t)}$ is the wet-bulb temperature at time t (K). Values of precipitation (P, cm) at time t and location x were found from estimates of snowfall (S, cm) by

$$P_{x,t} = S_{x,t} \times \frac{\rho_{ns(t)}}{p_w} \qquad (9)$$

where ρ_w is the density of liquid water (kg m^{-3}).

REFERENCES

Anderson EA. 1976. A point energy and mass balance model of a snow cover. NWS Technical Report **19**.

Bales R, Molotch N, Painter T, Dettinger M, Rice R, Dozier J. 2006. Mountain hydrology of the western United States. *Water Resources Research* **42**: W08432. DOI: 08410{DH}0102902005WR004387.

Bentz BJ, Allen CD, Ayres M, Berg E, Carroll A, Hansen M, Hicke J, Joyce L, Logan J, MacFarlane W, MacMahon J, Munson S, Negron J, Paine T, Powell J, Raffa K, Régnière J, Reid M, Romme W, Seybold S, Six D, Tomback D, Vandygriff J, Veblen T, White M, Witcosky J, and Wood D. 2009. In *Bark Beetle Outbreaks in Western North America: Causes and Consequences*, Bentz BJ (ed). Univ. of Utah Press: Salt Lake City, UT, ISBN: 978-0-87480965-7, 42 pp.

Bethlahmy N. 1974. More streamflow after a bark beetle epidemic. *Journal of Hydrology* **23**: 185–189.

Bethlahmy N. 1975. A Colorado episode: beetle epidemic, ghost forests, more stream flow. *Northwest Science* **49**(2): 95–105.

Boon S. 2007. Snow accumulation and ablation in a beetle-killed pine stand, northern Interior British Columbia. *BC Journal of Ecosystems and Management* **8**(3): 1–13.

Boon S. 2009. Snow ablation energy balance in a dead forest stand. *Hydrological Processes* **23**: 2600–2610.

Bowling DR, Massman WJ, Schaeffer SM, Burns SP, Monson RK, Williams MW. 2009. Biological and physical influences on the carbon isotope content of CO2 in a subalpine forest snowpack, Niwot Ridge, Colorado. *Biogeochemistry* **95**(1): 37–59. DOI: 10.1007/s105333-00809233-4.

Brooks PD, Williams MW, Schmidt SK. 1996. Microbial activity under alpine snowpacks, Niwot Ridge, CO. *Biogeochemistry* **32**: 93–113.

Brooks PD, Williams MW, Schmidt SK. 1998. Soil inorganic N and microbial biomass dynamics before and during spring snowmelt. *Biogeochemistry* **43**: 1–15.

Campbell GS, Norman JM. 1989. The description and measurement of plant canopy structure. In *Plant Canopies: Their Growth, Form and Function*, Russell G, Marshall B, Jarvis PG (eds). Cambridge University Press: Cambridge; 1–19.

Coléou C, Pieritz RA, Lseaffre B, Brzoska JB. 2004. Isothermal metamorphism of a new snow layer: snow measurements and simulation. Proceedings of the 2004 International Snow Science Workshop, Jackson Hole, Wyoming. 75–82.

Faria DA, Pomeroy JW, Essery RLH. 2000. Effect of covariance between ablation and snow water equivalent on depletion of snow-covered area in a forest. *Hydrological Processes* **14**: 2683–2695.

Fassnacht SR, Soulis ED. 2002. Implications during transitional periods of improvements to the snow processes in the Land Surface Scheme-Hydrological Model WATCLASS. *Atmosphere-Ocean* **40**(4): 389–403.

Fassnacht SR, Toro M, Simonson S, Bentley EK. 2006. From the tree to the forest-investigating snow accumulation around individual trees. Proceedings of the 2006 International Snow Science Workshop, Telluride, Colorado: 876–879.

Frankenstein S, Sawyer A, Koeberle J. 2008. Comparison of FASST and SNTHERM in three snow accumulation regimes. *Cold Land Processes Experiment: Special Collection*. DOI: 10.1175/2008JHM865.1.

Frazer GW, Canham CD, Lertzman KP. 1999. Gap Light Analyzer (GLA), Version 2.0: imaging software to extract canopy structure and gap light transmission indices from true-colour fisheye photographs, users manual and program documentation. Burnaby: Simon Fraser University and Millbrook: Institute of Ecosystem Studies.

Ge Y, Gong G. 2010. Land surface insulation response to snow depth variability. *Journal of Geophysical Research* **115**. DOI: 10.1029/2009JD012798.

Hardy JP, Davis RE, Jordan R, Li X, Woodcock C, Ni W, McKenzie JC. 1997. Snow ablation modeling at the stand scale in a boreal jack pine forest. *Journal of Geophysical Research* **102**(N24): 29, 397–29, 406.

Hardy JP, Melloh R, Robinson P, Jordan R. 2000. Incorporating effects of forest litter in a snow process model. *Hydrological Processes* **14**(18): 3227–3237.

Hardy JP, Melloh R, Koenig G, Marks D, Winstral A, Pomeroy JW, Link T. 2004. Solar radiation transmission through conifer canopies. *Agricultural and Forest Meteorology* **126**(3-4): 257–270. DOI: 10.1016/j.agrformet.2004.06.012.

Hedstrom NR, Pomeroy JW. 1998. Measurements and modelling of snow interception in the boreal forest. *Hydrological Processes* **12**: 1611–1625.

Hellström RA. 2000. Forest cover algorithms for estimating meteorological forcing in a numerical snow model. *Hydrological Processes* **14**: 3239–3256.

Hendrick RL, Rilgate BD, Adams WM. 1971. Application of environmental analysis to watershed snowmelt. *Journal of Applied Meteorology* **10**: 418–429.

Hirose T. 2005. Development of the Monsi-Saeki theory on canopy structure and function. *Annals of Botany* **95**: 483–494. DOI: 10.1093/aob/mci047.

Jenkins MJ, Hbertson E, Page W, Jorgensen CA. 2008. Bark beetles, fuels, fires and implications for forest management in the Intermountain West. *Forest Ecology and Management* **254**: 16–34.

Jordan R. 1991. A one-dimensional temperature model for a snow cover: technical documentation for SNTHERM89. Special Report 91-16. US Army Corps of Engineers, Cold Regions Research and Engineering Laboratory: Hanover, NH.

LaChapelle ER. 1969. *Field Guide to Snow Crystals*. University of Washington Press: Seattle, WA; 101 pp.

Lewis D, Huggard D. 2010. A model to quantify effects of Mountain Pine Beetle on equivalent clearcut area. *Streamline Watershed Management Bulletin* **13**(2): 42–51.

Link T, Marks D. 1999. Distributed simulation of snowcover mass- and energy-balance in the boreal forest. *Hydrological Processes* **13**: 2439–2452.

Liston GE, Elder K. 2006. A distributed snow-evolution modeling system (SnowModel). *Journal of Hydrometeorology* **7**: 1259–1276.

McNamara JP, Chandler D, Seyfried M, Achet S. 2005. Soil moisture states, lateral flow, and streamflow generation in a semi-arid, snowmelt-driven catchment. *Hydrological Processes* **19**: 4023–4038. DOI: 10.1002/hyp.5869.

Melloh RA, Hardy JP, Bailey R, Hall T. 2002. An efficient snow albedo model for the open and sub-canopy. *Hydrological Processes* **16**(18): 3571–3584.

Metcalfe RA, Buttle JM. 1998. A statistical model of spatially distributed snowmelt rates in a boreal forest basin. *Hydrological Processes* **12**: 1701–1722.

Molotch N, Brooks P, Burns S, Litvak M, Monson R, McConnel J, Musselman K. 2009. Ecohydrologic controls on snowmelt partitioning in mixed-conifer sub-alpine forests. *Ecohydrology* **2**: 128–142.

Monsi M, Saeki T. 1953. Uber den lichtfaktor in den pflanzengesellschaften end seine bedeutung fur die stoffproduktion. *Japanese Journal of Botany* **14**: 22–52.

Monson RK, Lipson DA, Turnipseed AA, Burns SP, Delany A, Williams MW, Schmidt SK. 2006. Winter forest soil respiration controlled by climate and community composition. *Nature* **439**: 711–714.

Monson RK, Prater MR, Hu J, Burns SP, Sparks JP, Sparks KL, Scott-Denton LE. 2010. Tree species effects on ecosystem water use efficiency in a high elevation subalpine forest. *Oecologia* **162**: 491–504.

Musselman KN, Molotch NP, Brooks PD. 2008. Effects of vegetation on snow accumulation and ablation in a mid-latitude sub-alpine forest. *Hydrological Processes* **22**: 2767–2776.

Musselman KN, Molotch NP, Margulis SA, Lehning M, Gustafsson D. 2012. Improved snowmelt simulations with a canopy model forced with photo-derived direct beam canopy transmissivity. *Water Resources Research.* DOI: 10.1029/2012WR012285.

Painter TH, Molotch N, Cassidy M, Flanner M, Steffen K. 2007. Contact spectroscopy for the determination of stratigraphy of snow grain size. *Journal of Glaciology* **53**(180): 121–127.

Pomeroy JW, Gray DM, Hedstrom NR, Janowicz JR. 2002. Physically based estimation of seasonal snow accumulation in the boreal forest. Proceedings, 59th Eastern Snow Conference. Stowe. 93–108.

Pomeroy J, Rowlands A, Hardy J, Link T, Marks D, Essery R, Sicart JE, Ellis C. 2008. Spatial variability of shortwave irradiance for snowmelt in forests. *Journal of Hydrometeorology* **9**: 1482–1490.

Pomeroy JW, Marks D, Link T, Ellis C, Hardy J, Rowlands A, Granger R. 2009. The impact of coniferous forest temperature on incoming longwave radiation to melting snow. *Hydrological Processes*, **23**(17): 2513–2525. DOI: 10.1002/hyp.7325.

Potts DF. 1984. Hydrologic impacts of a large scale mountain pine beetle (*Dendroctonus ponderosae* Hopkins) epidemic. *Water Resources Bulletin* Paper No. 83122, **20**: 373–377.

Pugh ET, Gordon ES. 2012. A conceptual model of water yield impacts from beetle-induced tree death in snow-dominated lodgepole pine forests. *Hydrological Processes.* DOI: 10.1002/hyp.9312.

Pugh ET, Small EE. 2011. The impact of pine beetle infestation on snow accumulation and melt in the headwaters of the Colorado River. *Ecohydrology* **4**: n/a. DOI:10.1002/eco.23.

Pugh ET, Small EE. 2012. The impact of beetle-induced conifer death on stand-scale canopy snow interception. *Hydrology Research*, submitted May 2012, in review.

Rutter N, Essery R, Pomeroy J, Altimir N, Andreadis K, Baker I, Barr A, Bartlett P, Boone A, Deng H, Douville H, Dutra E, Elder K, Ellis C, Feng X, Gelfan A, Goodbody A, Gusev Y, Gustafsson D, Hellström R, Hirabayashi Y, Hirota T, Jonas T, Koren V, Kuragina A, Lettenmaier D, Li W, Luce C, Martin E, Nasonova O, Pumpanen J, Pyles RD, Samuelsson P, Sandells M, Schädler G, Shmakin A, Smirnova TG, Stähli M, Stöckli R, Strasser U, Su H, Suzuki K, Takata K, Tanaka K,

Thompson E, Vesala T, Viterbo P, Wiltshire A, Xia K, Xue Y, Yamazaki T. 2009. Evaluation of forest snow processes models (SnowMIP2). *Journal of Geophysical Research* **114**. DOI: 10.1029/2008JD011063.

Sicart JE, Pomeroy JW, Essery RE, Hardy J, Link T, Marks D. 2004. A sensitivity study of daytime net radiation during snowmelt to forest canopy and atmospheric conditions. *Journal of Hydrometeorology* **5**: 774–784.

Tague C. 2006. Heterogeneity in hydrologic processes: a terrestrial hydrologic modeling perspective. Ecosystem function in heterogeneous landscapes, pp. 119–136.

Tarboton DG, Luce CH. 1996. Utah energy balance snow accumulation and melt model (UEB), computer model technical description and users guide. Logan: Utah Water Res. Lab.

Varhola A, Coops NC, Weiler M, Moore RD. 2010. Forest canopy effects on snow accumulation and ablation: an integrative review of empirical results. *Journal of Hydrology* **319**: 219–233.

Veatch W, Brooks PD, Gustafson J, Molotch NP. 2009. Quantifying the effects of forest canopy cover on net snow accumulation at a continental, mid-latitude site, Valles Caldera National Preserve, NM, USA. *Ecohydrology* **2**. DOI: 10.1002/eco.45.

Westerling AL, Hidalgo HG, Cayan DR, Swetnam TW. 2006. Warming and earlier spring increases Western U.S. forest wildfire activity. *Science* **313**: 940–943. DOI: 10.1126/science.1128834.

Williams MW, Seibold C, Chowanski K. 2009. Storage and release of solutes from a subalpine seasonal snowpack: soil and stream water response, Niwot Ridge, Colorado. *Biogeochemistry* **95**: 77–94. DOI: 10.1007/s10533-009-9288-x.

Winkler RD, Spittlehouse DL, Golding DL. 2005. Measured differences in snow accumulation and melt among clearcut, juvenile, and mature forests in southern British Columbia. *Hydrological Processes* **19**: 51–62. DOI: 10.1002/hyp.5757.

Winkler R, Boon S, Zimonick B, Baleshta K. 2010. Assessing the effects of post-pine beetle forest litter on snow albedo. *Hydrological Processes* **24**: 803–812.

Wulder MA, White JC, Bentz B, Alvarez MR, Coops NC. 2006. Estimating the probability of mountain pine beetle red-attack damage. *Remote Sensing of Environment* **101**: 150–166.